QUANTITATIVELY IDENTIFY UNSTEADY GAS POLLUTANT RELEASES BY INVERSE CFD MODELING

Shi Yin, Tengfei (Tim) Zhang, Shugang Wang, and Yue Zhao
School of Civil Engineering, Dalian University of Technology (DUT)
2 Linggong Rd, Dalian 116024, China

ABSTRACT

This study proposed the Tikhonov regularization strategy coupled with the least-squares optimization to identify unsteady gas release processes from a fixed spot. The Tikhonov regularization adds a regularized term to the optimizing objective function and imposes a bound to solution. To accelerate the solving procedure, the unsteady gas concentration is calculated as the convolution integral between the concentration response by a unit impulse release and the arbitrary unsteady release. It finds the developed inverse model can accurately and efficiently quantify the unsteady gas release either in a constant or sinusoidal form for a while in a square ventilation cavity.

INTRODUCTION

In case airborne hazards are accidentally released indoors, it is always helpful to know where and how the pollutants have been released. Thereafter, emergency actions can be appropriately taken to protect indoor occupants from being harmed. To identify an unknown pollutant release event, some detection sensors shall be deployed. However, when the sensor alarms the accidental release of a hazardous pollutant, the event has already happened. An intuitive method to determine the source location and identify the unsteady release scenario is by recovering the pre-occurring process from the time of sensor alarming until to the moment of initial release. Such forms the framework of the so-called inverse modeling, i.e., finding some unknown causal information based on a limited amount of detected consequences.

The current inverse modeling is able to determine the pollutant source location. Zhang and Chen (2007) developed both the quasi-reversibility and pseudo-reversibility models to successfully locate an instantaneous gas source. The quasi-reversibility model reverses the time marching direction of the governing equation and improves the solution stability by replacing the second-order diffusion term with a fourth-order stabilization term. The pseudo-reversibility model solves the convection transport of pollutant based on the reversed flow field. Later, the quasi-reversibility model is extended into identify a particulate source after including the gravitational settling effect, and the Lagrangian-reversibility model is proposed to circumscribe a particulate source with discrete track particles (Zhang et al., 2011). With a similar operation to reverse the flow field, Liu and Zhai (2008) developed the adjoint method to locate an instantaneous point source indoors. The backward-in-time pollutant plume location and travel time probabilities are found to be adjoint states of the forward-in-time local pollutant concentration. After solving the adjoint probability equation, the likelihood of a pollutant source location can be predicted. The above inverse models are solved by computational fluid dynamics (CFD), so the accuracy is generally good.

In common situation, if there is no rigor demand in identification accuracy, one may turn to the more efficient multi-zone model. Sohn et al. (2002) developed a data-interpretation model based on the Bayesian-probability to search for a location and release scenario in a pre-established database, trying to find a solution that best matches with the measurement concentration. The database presumes all possible source locations and release scenarios, and then simulates and stores the concentration information accordingly. Such interpretative strategy based on probability is further extended to establish a systematic sensor network (Sreedharan et al. 2006). Similarly with the multi-zone model, Vukovic et al. (2010) proposed to find an indoor pollutant source based on the optimization of the artificial neural network. The release scenario of pollutant sources is assumed to be known, so interpreting result in real time can be realized.

However, in practice the release scenario of a pollutant source is unknown and the unsteady release process can be very complicated. It may be very hard to enumerate all possible pre-event scenarios to establish a complete database, though the multi-zone models are efficient. On the other hand, the aforementioned inverse CFD modeling should be able to catch the pollutant source location but cannot quantify the complicated unsteady release process. This paper thus presents the inverse fundamentals to identify the unsteady release process of a gaseous pollutant source based on CFD, by assuming the

release is from a known fixed location in a steady flow field.

INVERSE MODELS

The current sensor system can respond discrete gas pollutant concentration at the measurement locations, and such concentration information is treated as the known inputs to infer the unsteady release process. Suppose the steady flow filed is available, the core task of inverse modeling is to find a release scenario that best matches with the provided measurement concentration. Assume the concentration distribution and the unsteady gas release satisfies the following relation,

$$\boldsymbol{c}=\boldsymbol{A}\boldsymbol{q} \tag{1}$$

where $\boldsymbol{c}=\left[C_{t_0},\ldots,C_{t_k},\cdots,C_{t_n}\right]^T$ is the concentration vector at discrete time t_k at the measurement spot, $\boldsymbol{q}=\left[q_{t_0},\cdots,q_{t_k},\cdots,q_{t_n}\right]^T$ is the gas release strength, $\boldsymbol{A}$ is a matrix that describes the cause-effect relation between the release strength and the exhibited concentration. Such cause-effect relation is governed by the gaseous pollutant transport equation,

$$\frac{\partial(\rho C)}{\partial t}+\frac{\partial}{\partial x_i}\left[(\rho u_i C)\right]=\frac{\partial}{\partial x_i}\left[\Gamma\frac{\partial C}{\partial x_i}\right]+\boldsymbol{q} \tag{2}$$

where ρ is air density, C is unsteady pollutant concentration, t is time, x_i (i=1, 2, 3) is the position in the Cartesian coordinates, u_i (i=1, 2, 3) is the air velocity component, and Γ is the effective diffusivity. If the pollutant source location is fixed, the concentration varies linearly with the release strength at a fixed spot, i.e., $\boldsymbol{A}$ would be a linear matrix.

The inverse determination of the unsteady release process is to solve for the vector $\boldsymbol{q}$ based on equation (1). If the solution is optimized by the linear least squares scheme, the task is to find a $\boldsymbol{q}$ that can minimize the residual fucntion Z as,

$$Z(\boldsymbol{q})=\left\|\boldsymbol{A}\boldsymbol{q}-\boldsymbol{c}\right\|_2^2 \tag{3}$$

The above equation weighs the difference between the measured concentration ($\boldsymbol{c}$) and the calculated concentration based on the cause-effect relation ($\boldsymbol{Aq}$). Generally, by minimizing the residual equation (3), the release vector $\boldsymbol{q}$ can be solved. However, equation (3) is ill-posed because matrix $\boldsymbol{A}$ cannot be inversed. This paper adopts the well-known Tikhonov Regularization (Tikhonov et al., 1977) to change the ill-posed problem into a well-posed problem. Based on the Tikhonov regularization, the objective residual is defined as,

$$Z(\boldsymbol{q})=\left\|\boldsymbol{A}\boldsymbol{q}-\boldsymbol{c}\right\|_2^2+\lambda^2\left\|\boldsymbol{L}\boldsymbol{q}\right\|_2^2 \tag{4}$$

By differentiating the above equation with respect to $\boldsymbol{q}$ and setting it to zero, the corresponding $\boldsymbol{q}$ when minimizing equation (4) is,

$$\boldsymbol{q}=(\boldsymbol{A}^T\boldsymbol{A}+\lambda^2\boldsymbol{L}^T\boldsymbol{L})^{-1}\times(\boldsymbol{A}^T\boldsymbol{c}) \tag{5}$$

where λ is the regularization parameter that controls the relative strength of the regularization operator $\boldsymbol{L}$. The most popular form of $\boldsymbol{L}$ is an N-th order derivative operator,

$$\left\|\boldsymbol{L}\boldsymbol{q}\right\|^2\approx\int_0^t\left(\frac{d^N\boldsymbol{q}}{dt^N}\right)^2dt \tag{6}$$

For a smooth solution, a typical choice is N=2. Therefore, $\boldsymbol{L}$ can be expressed by (Hansen, 1997),

$$\boldsymbol{L}=\begin{bmatrix}1&-2&1&0&0&\ldots\\0&1&-2&1&0&\ldots\\0&0&1&-2&1&\ldots\\\vdots&\vdots&\vdots&\vdots&\vdots&\vdots\end{bmatrix}\in R^{(n-2)\times n} \tag{7}$$

Choosing a suitable λ becomes the core of the Tikhonov regularization. One effective method to find an optimal λ is by applying the L-curve approach. The L-curve presents the norm of regularized term ($\boldsymbol{Lq}$) versus the norm of residual term ($\boldsymbol{Aq}$-$\boldsymbol{c}$) in the log-log coordinate for a sequence of λ. The L-curve can be smoothed by the cubic spline as recommended by Hansen (1997). The regularization parameter λ when obtaining the maximum curvature on the L-curve is often the optimal choice. The L-curve is defined as,

$$(X(\log\lambda),Y(\log\lambda))=(\log\left\|\boldsymbol{A}\boldsymbol{q}-\boldsymbol{c}\right\|_2,\log\left\|\boldsymbol{L}\boldsymbol{q}\right\|_2) \tag{8}$$

and its curvature is,

$$\kappa(\log\lambda)=\frac{X'Y''-X''Y'}{((X')^2+(Y')^2)^{(3/2)}} \tag{9}$$

where the differentiation in equation (9) is with respect to logλ. The L-curve criterion is to find the λ(logλ) that matches with the curvature maximization.

So far there is still lack of the explicit form of the matrix $\boldsymbol{A}$. If the governing equation (2) is solved for concentration response for each release strength, the optimization will be computationally prohibited. Fortunately, when the release location is fixed, matrix $\boldsymbol{A}$ is linear. The concentration from an arbitrary release can be expressed as the convolution integral between the unsteady release and the concentration response of a unit impulse release as,

$$\boldsymbol{c}(t)=\boldsymbol{A}\boldsymbol{q}(t)=\int_{-\infty}^{+\infty}\boldsymbol{q}(\tau)\left\{\boldsymbol{A}\delta\left(t-\tau\right)\right\}d\tau \tag{10}$$

where $\boldsymbol{q}(\tau)$ is an arbitrary release function over time, $\delta(t-\tau)$ is a unit impulse release. The discrete

format of the concentration at a certain point can be expressed as (Ishida and Kato, 2007),

$$C_n = \sum_{k=0}^{\infty} q_k F_{n-k} = q_0 F_n + q_1 F_{n-1} + \cdots + q_k F_{n-k} + \cdots + q_\infty F_{n-\infty} \quad (11)$$

where C_n is the concentration at n time step at a location, q_k is the arbitratry release strength at k time step, and F_{n-k} is the local cocentration response at (n-k) time step from a unit impulse release, which is also called the local concentration response factor (Ishida and Kato, 2007).

By comparing equation (11) with equation (10), it can be seen that the time step (ΔT) is removed in equation (11). Hence, the concentration response factor shall take into account ΔT. For convenience, the unit impulse release process is defined as an isoceles triangle as shown in Figure 1, which spans $2\Delta T$. The total rate by the unit impulse release would be (1unit·ΔT).

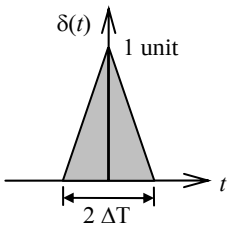

Figure 1 The defined unit impulse release scenario

DESCRIPTION OF TEST CASES

For demonstrating the inverse modeling, this investigation has designed several unsteady gas release scenarios in a two-dimensional square cavity as shown in Figure 2. Conditioned air at 15 °C is supplied in from a slot inlet located at the upper-left corner, while the inside air is extracted by an exhaust at the lower-right corner. Except for the bottom surface that is maintained at 35.5 °C, other walls of this cavity are controlled to be 15 °C.

Two gas source locations are designed: one is at the air supply; the other is at the cavity centre. This investigation tests two unsteady release forms: either a constant release for a while or the release following the sinusoidal curve for a cycle over time. The combinations between different gas source locations and release scenarios constitute four test cases as shown in Table 1. In Cases 1 and 2, the source is at the air supply inlet, while the gas source releases at the cavity centre in Cases 3 and 4. The detailed unsteady release process in each case is illustrated in Figure 3.

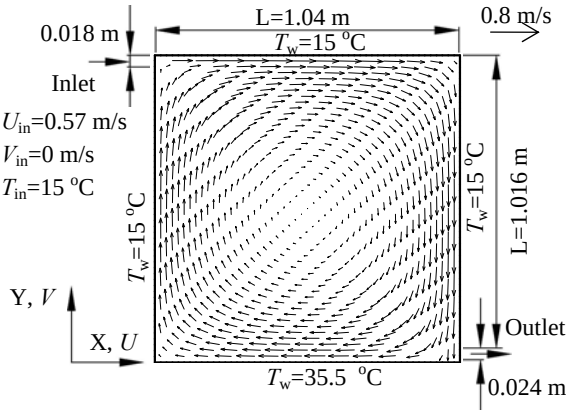

Figure 2 A two-dimensional square cavity to test the inverse model

Before conducting inverse modeling, the inside airflow and measurement concentation at the monitoring point shall be provided. This investigation has applied the forward CFD modeling to obtain the required information. The inside airflow is governed by a set of partial differential Navier-Stokes equations including fluid continuity, momentum and energy. To resolve flow turbulence, the Reynolds-averaged approach is applied, and the random turbulence effect is approximated by the RNG k-ε turbulence model. Once the flow is solved, the flow is frozen for unsteady gas dispersion modeling. In addition to gas concentration distribution, the corresponding concentration response factor by a unit impulse release is also solved. A commercial CFD software, FLUENT, is applied to carry out the forward simulation.

Table 1
The designed test cases

Case	Source location	Release form
1	Inlet	Constant for 3 s
2	Inlet	One sinusoidal cycle for 4 s
3	Cavity centre	Constant for 10 s
4	Cavity centre	One sinusoidal cycle for 20 s

Figure 2 presents the solved flow pattern inside the cavity. The flow generally goes clockwise and forms a big vortex in the centre. This internal airflow is under forced convection. Figure 4 illustrates the unsteady gas concentration at the outlet for each case. The concentration decays cycle by cycle in Cases 1 and 2, but gradually increases in Cases 3 and 4. Figure 5 shows the concentration response at the outlet by the unit impulse release when the source is at the inlet and cavity centre, respectively. The time step (ΔT in Figure 1) for impulse release is 0.1 s. However, to obtain the unsteady concentration response with a high resolution, the time step in solving equation (2) is 0.01 s.

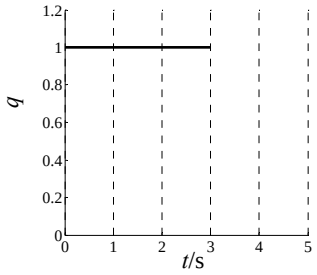

(a) Case 1 (at the inlet)

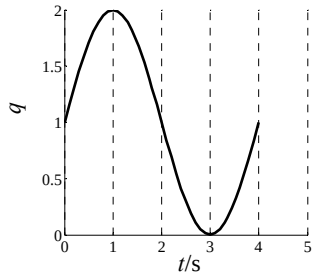

(b) Case 2 (at the inlet)

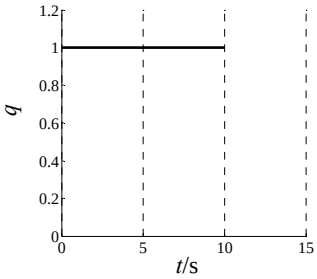

(c) Case 3 (at the cavity centre)

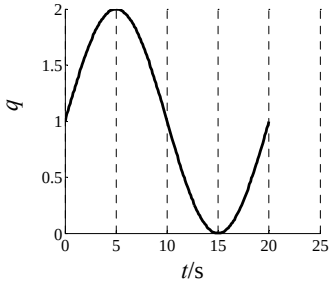

(d) Case 4 (at the cavity centre)
Figure 3 Unsteady release process in each case

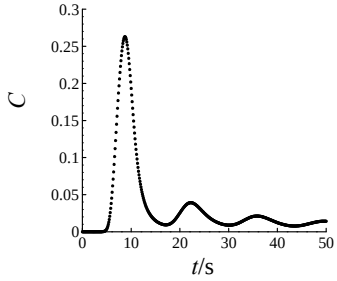

(a) Case 1 (Constant release at the inlet)

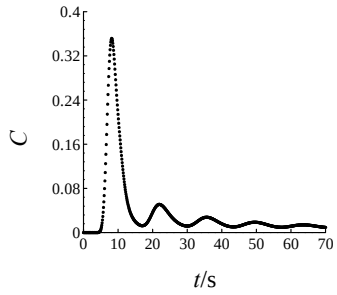

(b) Case 2 (Sinusoidal release at the inlet)

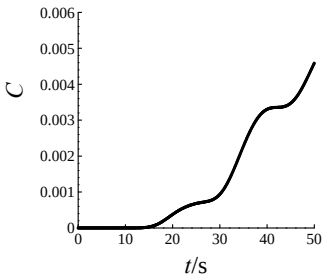

(c) Case 3 (Constant release at the cavity centre)

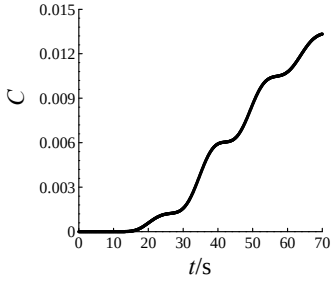

(d) Case 4 (Sinusoidal release at the cavity centre)
Figure 4 The discrete concentration over time at the cavity outlet

The monitored discrete concentration over time at the cavity outlet as shown in Figure 4 and the steady flow field in Figure 2, are the given known information to conduct inverse modeling. The unit impulse concentration response as shown in Figure 5 will be used to reconstruct the cause-effect relation between release strength and concentration.

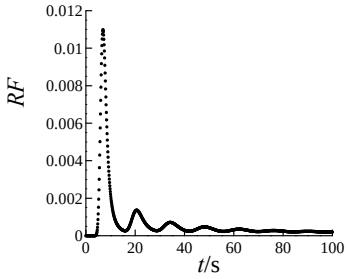

(a) Release at the air supply inlet

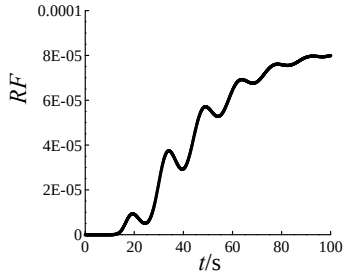

(b) Release at the cavity centre

Figure 5 The unit impulse concentration response (RF) at the cavity outlet

RESULTS AND DISCUSSIONS

The inverse identification is carried out by a self-developed program in MATLAB. After optimizing equation (4) based on the measured discrete concentration, the release strength vector, $\boldsymbol{q}$, can be provided.

Case 1 (Constant release at the inlet)

With a time step of 0.1 s and the monitoring duration of 50 s, the concentration vector $\boldsymbol{c}$ has the form of $\boldsymbol{c} \in R^{501\times1}$ and coefficient matrix $\boldsymbol{A} \in R^{501\times501}$. Here we suppose the contaminant release and concentration monitoring are synchronous.

As previously mentioned, the key to solve inverse modeling is to find a suitable regularized parameter, λ. We tested different λ in a geometric sequence, starting from 1.0e-5 to 1.4458 with an increasing ratio of 1.02. Figure 6(a) shows the L-curve, which is calculated based on equation (8). The relative weight ratio between the original optimizing term and the regularized term varying with λ can be viewed. The curvature κ of the L-curve with respect to $\log\lambda$ is shown in Figure 6(b), which is plotted based on equation (9). Here λ starts from 3.9211e-5 ($\log\lambda$=-4.41), rather than the initial value of 1.0e-5. This is because when λ is very small, the inverse solution becomes very sensitive to the regularization parameter. The peaks, C_1, C_2, C_3, C_4 and C_5, indicate the inflexion points on the L-curve. Figure 6(c) presents the true error (q_{error}) versus $\log\lambda$. q_{error} refers to the difference between the recovered release strength and the realistic release with the expression of,

$$q_{\text{error}} = \left\| \boldsymbol{q}_{\text{ture}} - \boldsymbol{q}_{\text{recovered}} \right\|_2 \tag{12}$$

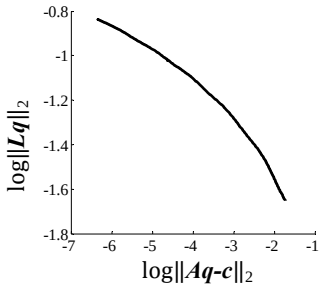

(a)

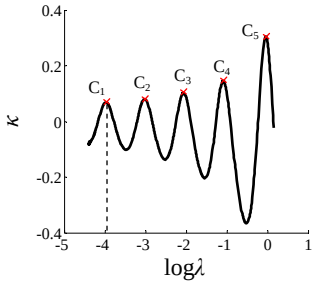

(b)

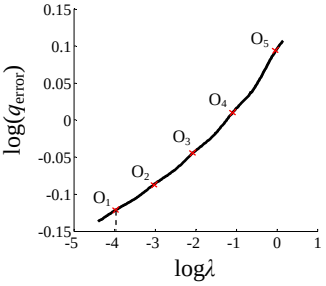

(c)

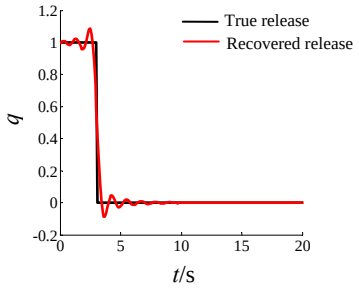

(d)

Figure 6 Identified unsteady release for Case 1 (a) linear L-curve, (b) curvature versus logλ, (c) true error versus logλ and (d) recovered release rate versus time for initial 20 s

Obviously, C_1, C_2, C_3, C_4 and C_5 are the five possible optimal regularization parameters, and O_1, O_2, O_3, O_4 and O_5 indicate their corresponding true errors. O_1 is the point where the true error is the minimum so that the regularization parameter at point O_1 is the optimum between these five choices. Hence, the optimal regularization parameter is taken as λ=1.0554e-4 ($\log\lambda$=-3.9766). Figure 6(d) shows recovered release strength versus time and the

comparison with the actual release scenario. For viewing clearly, only the result within the initial 20 s is displayed. In the later 30 s, the recovered release strength is nearly identical to the actual release.

From Figure 6(d), it can be seen there are some oscillations in the recovered release for the initial 3 s. However, the amplitude of the oscillation can be controlled within 10% of the baseline value. The realistic release suddenly stops after t=3 s. The inverse modeling can right catch the trend of such sharp change. Though some oscillations emerge within 0~3 s, the overall agreement of these two processes is quite good. This attests to the good performance of the proposed inverse modeling strategy.

It shall point out during the practical use, the true release is unknown, so λ shall be selected based on Figure 6(b) rather than from Figure 6(c). We have tested other λs on C_2, C_3, C_4 and C_5, and found they generally work. However, when λ increases, the generated oscillation also increases. Besides, as we searched for λ only within a limited range instead of the whole distribution, the provided λ might be only a local optimal parameter. It is possible there exists such a λ, which may provide better result than that shown in Figure 6(d).

Case 2 (Sinusoidal release at the inlet)

In case 2, the contaminant source releases for 4 s in a sinusoidal form (Figure 3(b)). The concentration is monitored at the outlet from t=0 to 70 s. With the same time step of 0.1 s, the concentration has a dimension of $\boldsymbol{c} \in R^{701\times1}$ and coefficient matrix of $\boldsymbol{A} \in R^{701\times701}$.

Again, λ is tested based on a geometric sequence from 1.0e-5 to 1.4458 with an increasing ratio of 1.02. Figure 7(a) plots the L-curve. Its curvature versus logλ is shown in Figure 7(b), where λ starts from 3.9211e-5 (logλ=-4.4066). Similar to Case 1, the peaks C_1, C_2, C_3 and C_4 indicate the inflexion points of the L-curve and thus are possible choices for the optimal regularization parameters. O_1, O_2, O_3 and O_4 indicate the corresponding true errors as shown in Figure 7(c). Among them, O_1 is the point with the minimum error. Therefore, λ=6.6929e-5 (logλ=-4.1744) at C_1 (O_1) is adopted for inverse release recovering.

The comparison between the recovered unsteady release and the true release for the previous 20 s is shown in Figure 7(d). It shows that the recovered and true releases have excellent agreement in the initial 3.5 s. The recovered release captures the first release peak clearly and accurately. However, the second peak is only a half of the true release. The underlying possible reason is the concentration response delay or insufficient monitoring data that results in some unknown identification uncertainty.

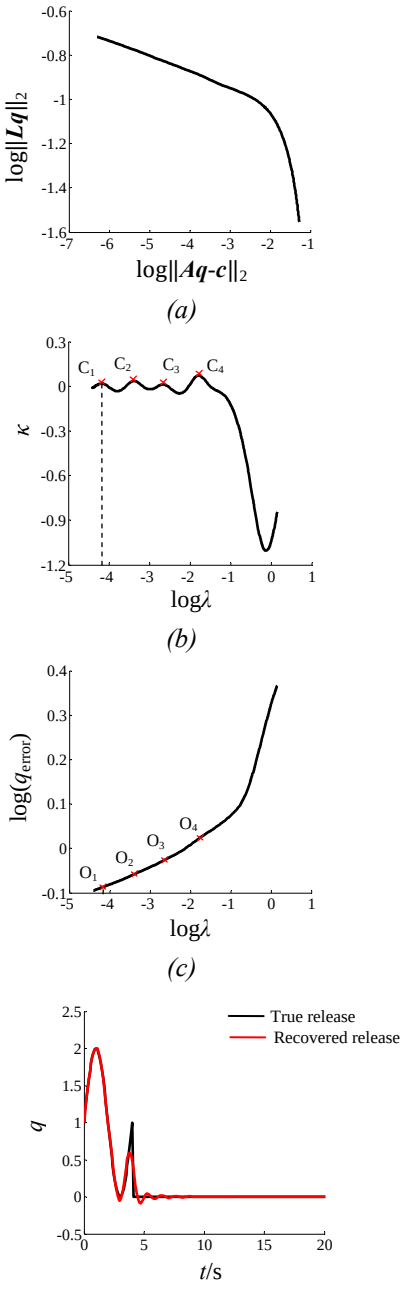

Figure 7 Identified unsteady release for Case 2 (a) linear L-curve, (b) curvature versus logλ, (c) true error versus logλ and (d) recovered release rate versus time for initial 20 s

Case 3 (Constant release at the cavity centre)

In case 3, the contaminant source releases for 10 s at a constant rate (Figure 3(c)). The concentration is monitored at the outlet from t=0 to 50 s. With the same time step of 0.1 s, the concentration has a dimension of $\boldsymbol{c} \in R^{501\times1}$ and coefficient matrix of $\boldsymbol{A} \in R^{501\times501}$

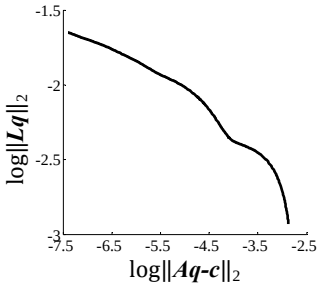

(a)

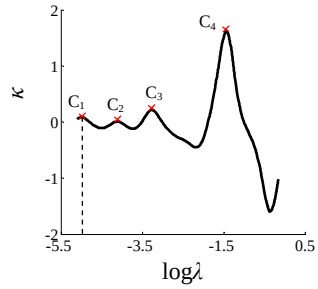

(b)

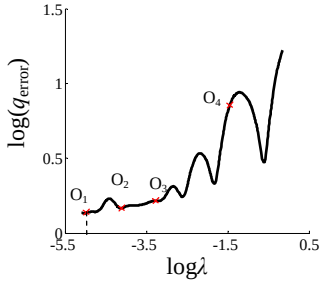

(c)

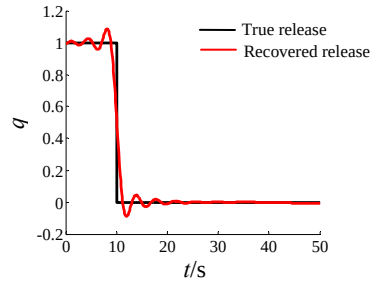

(d)

Figure 8 Identified unsteady release for Case 3 (a) linear L-curve, (b) curvature versus logλ, (c) true error versus logλ and (d) recovered release rate versus time

Similar to the previous cases, the L-curve, curvature of the L-curve and true errors are plotted in Figure 8(a), (b), (c), respectively. λ ranges from 5.0e-6 to 0.7229 with an increasing ratio of 1.02. The true error at O_1 is the minimum, so the regularization parameter at O_1 is the optimal value. Therefore, we selected λ=1.0403e-5 (logλ=-4.9828) at C_1 (O_1) for inverse release identification.

The recovered unsteady release process is compared with the true release process in Figure 8(d). Similar to case 1, some oscillations exist. However, the amplitude of oscillation is within 10% of the actual baseline value.

Case 4 (Sinusoidal release at the cavity centre)

The source releases for 20 s in a sinusoidal form (Figure 3(d)) in Case 4. With the monitoring duration of 70 s and a time step of 0.1 s, the concentration vector $\boldsymbol{c}$ holds the form of $\boldsymbol{c} \in R^{701\times1}$ and coefficient matrix $\boldsymbol{A} \in R^{701\times701}$.

Figure 9(a), (b) and (c) show the L-curve, curvature of L-curve and true errors of inversed solution, respectively. λ varies in a geometric sequence from 5.0e-6 to 0.7229 with an increasing ratio of 1.02. Here, O_1 with λ=4.2209e-4 (logλ=-3.3746) is the best choice because its error is the minimum.

Figure 9(d) shows the comparison between the recovered and the true release. The recovered and true release processes agree excellently before t=18 s. When the true release suddenly stops after t=20 s, the response in the recovered release lags behind a little bit. Though there is some difference in the second peak, the overall trend of the recovered release matches well with the actual process.

The above four cases are conducted in a personal computer with a frequency of 2.4G Hz and memory of 3.25GB. The computational time for inverse identification depends on the search range of λ as shown in Table 2. The third column lists the execution time for a big range of λ. It ranges from around one to three times of the acutual monitoring duration of the polluant release. However, if λ is limited to a small range but still including the optimal λ as listed in the last column of Table 2, the inverse identification can be fulfilled faster than the real time. The solution time for the local concentration response factor (by the unit impulse release) for 100 s is around 3.5 hours, but such computation can be carried out before the inverse identification. This indicates the proposed inverse identification is quite efficient.

Table 2
Cumputation time for each inverse identification

Case	Inverse duration	Calculating time for a big range of λ	Calculating time for a small range of λ
1	50 s	63 s (-5<logλ<0.16)	20 s (-5<logλ<-3.4)
2	70 s	143 s (-5<logλ<0.16)	46 s (-5<logλ<-3.4)
3	50 s	70 s (-5.3<logλ<-0.14)	24 s (-5.3<logλ<-3.4)
4	70 s	158 s (-5.3<logλ<-0.14)	55 s (-5.3<logλ<-3.4)

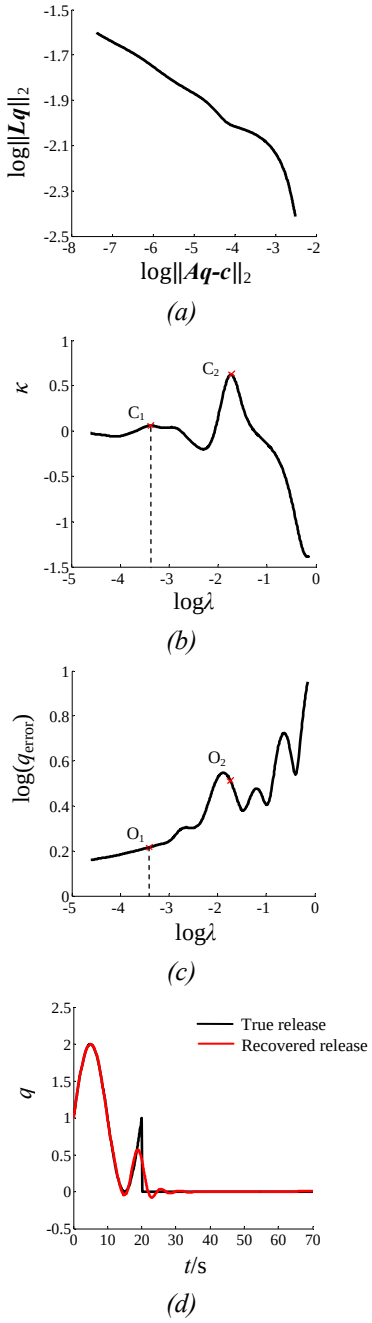

Figure 9 Identified unsteady release for Case 4 (a) linear L-curve, (b) curvature versus logλ, (c) true error versus logλ and (d) recovered release rate versus time

SUMMARY

This paper proposes an inverse modeling strategy to identify the complex unsteady release process from a fixed gaseous pollutant source. The Tikhonov Regularization is coupled with the least squares optimization to solve for the unsteady release strengths. To accelerate the solving procedure, the cause-effect relation between the release strength and concentration response is described by the convolution integral theory. The test results show the developed inverse model can quantify the complex release process accurately and efficiently. Though there are some oscillations when the release rate changes sharply, the generated error is within 10% of the baseline value. If the regularized parameter is limited to a small range, the inverse identification can be fulfilled faster than the real time, once the concentration response of a unit impulse release is pre-calculated. This shows the proposed inverse strategy is promising to be applied for emergency response when airborne hazards are accidentally released.

ACKNOWLEDGEMENT

This research work was supported by the National Natural Science Foundation of China (Grant No.: 50808028).

REFERENCE

Hansen, P.C. 1997. Rank-deficient and discrete ill-posed problem: Numerical aspects of linear inversion, Philadelphia, SIAM.

Ishida, Y., Kato, S. 2007. Method for coupling three-dimensional transient pollutant transport into one-dimensional transport simulation based on concentration response factor, ASHRAE Transactions, 114 (1), 259-272.

Liu X., Zhai Z. 2008. Location identification for indoor instantaneous point contaminant source by probability-based inverse computational fluid dynamics modeling, Indoor Air, 18 (1), 2-11.

Sohn, M.D., Reynolds, P., Singh, N. and et al. 2002. Rapidly locating and characterizing pollutant releases in buildings, Journal of Air & Waste Management Association, 52, 1422-1432.

Sreedharan, P., Sohn, M., Gadgil, A. and et al. 2006. Systems approach to evaluating sensor characteristics for real-time monitoring of high-risk indoor contaminant releases, Atmospheric Environment, 40, 3490-3502.

Tikhonov, A.N., Arsenin, V.Y. 1977. Solutions of ill-posed problems, Washington, DC, Halsted Press.

Vukovic, V., Tabares-Velasco, P.S., Srebric, J. 2010. Real-time identification of indoor pollutant source positions based on neural network locator of contaminant sources and optimized sensor networks, Journal of the Air & Waste Management Association, 60, 1034-1048.

Zhang T., Chen Q. 2007. Identification of contaminant sources in enclosed spaces by a single sensor, Indoor Air, 17(6), 439-449.

Zhang T., Li H., Wang S. 2011. Identification of particulate contaminant source locations in enclosed spaces with inverse CFD modelling, Proceeding of Indoor Air 2011, ID:278, 1-6.